Hindawi Publishing Corporation
Mathematical Problems in Engineering
Volume 2014, Article ID 620389, 13 pages
http://dx.doi.org/10.1155/2014/620389

Research Article

Numerical Research on Hydraulically Generated Vibration and Noise of a Centrifugal Pump Volute with Impeller Outlet Width Variation

Houlin Liu,[1] Jian Ding,[1,2] Hanwei Dai,[1] Minggao Tan,[1] and Xiaochen Tang[2]

[1] *Research Center of Fluid Machinery Engineering and Technology, Jiangsu University, Zhenjiang 212013, China*
[2] *Jiangsu Zhenhua Pump Industry Co., Ltd., Taizhou 225500, China*

Correspondence should be addressed to Jian Ding; jeremydin@gmail.com

Received 27 May 2014; Revised 22 August 2014; Accepted 10 September 2014; Published 12 October 2014

Academic Editor: Delfim Soares Jr.

The impeller outlet width of centrifugal pumps is of significant importance for numbers of effects. In the paper, these effects including the performance, pressure pulsations, hydraulically generated vibration, and noise level are investigated. For the purpose, two approaches were used to predict the vibration and sound radiation of the volute under fluid excitation force. One approach is the combined CFD/FEM analysis for structure vibration, and then the structure response obtained from the FEM analysis is treated as the boundary condition for BEM analysis for sound radiation. The other is the combined CFD/FEM/BEM coupling method. Before the numerical methods were used, the simulation results were validated by the vibration acceleration of the monitoring points on the volute. The vibration and noise were analyzed and compared at three flow conditions. The analysis of the results shows that the influences of the sound pressure of centrifugal pumps on the structure appear insignificant. The relative outlet width b_2^* at $n_q(\mathrm{SI}) = 26.7$ in this paper should be less than 0.06, based on an overall consideration of the pump characteristics, pressure pulsations, vibration and noise level.

1. Introduction

The volute pump type is perhaps the most common type of centrifugal pumps in the world. It is widely applied in industrial and civilian use. In these applications, the vibrations and noise problems are getting more and more attention. Both vibrations and noise can affect the centrifugal pump performance and its life. In centrifugal pumps, the sources of vibrations and noise may lie in hydraulic or mechanical aspects [1]. But, under normal operating condition, the blade passing frequency is the most usual excitation of vibrations and noise. The blade passing frequency (BPF) is represented as the product of the number of blades and rotation speed. Large BPF amplitude (and its harmonics) can lead to a lot of noise and vibrations, which may be the source of components wear and bearing failure [2]. This frequency is a consequence of the nonuniformity of the flow at the impeller outlet which is caused by the effects of the rotor-stator interaction.

The nonuniformity of the flow exiting the impeller is greatly affected by the impeller outlet width, according to the literature [3]. The turbulent dissipation losses in the collector increase with the nonuniformity of the flow at the impeller outlet. As a result, the pump performance and shaft power are affected. Studies have been conducted in order to improve the pump performance through optimizing the outlet width [4–6]. In respect of vibrations and noise, although these characteristics are expected to vary with the outlet width, the detailed studies have not been conducted. The current work is mainly to investigate the effects of the impeller outlet width on hydraulically generated vibration and noise of a centrifugal pump.

To do the investigation, the analysis model for vibrations and noise of centrifugal pumps should be developed at first. Most previous works have focused on theoretical and experimental studies [7–16]. Recently, the fluid-dynamic calculations combined with acoustic analogies have been developed.

In this method, acoustic sources are predicted from CFD calculations [17, 18] or a discrete vortex method [19, 20]. Then, the acoustic response is calculated by means of a boundary element method (BEM) [18, 21–23]. These studies seem to have simulated the hydroacoustic noise only, without the effects of structural vibrations being considered. Kato et al. [24] and Jiang et al. [25] conducted a fluid-structure weakly coupled simulation method to investigate the flow induced noise in pumps. There are three processes in the coupled simulation. The first step is still to obtain acoustic sources predicted from CFD simulation. Then, the dynamic response of structure under the excitation of pressure pulsations is simulated. Finally, the acoustical simulation is performed. However, in their simulations, the feedback effects of sound pressure on the structural vibration were neglected. In order to take the feedback effects into consideration, the coupled FEM/BEM algorithm was developed [26, 27]. However, the coupled approach concerning the vibration and noise problems of centrifugal pumps has not been reported in literature.

From the above discussions, we can come to the conclusion that there are mainly two approaches for pump vibration and noise simulation. One approach is the FEM analysis for structure vibration, and then the structure response obtained from the FEM analysis is treated as the boundary condition for BEM analysis for sound radiation. The other is the coupled FEM/BEM method. In present study, the two approaches are used. But for our problem, the excitation force is from the turbulence flow inside the pump, which is complicated and nonlinear. As such, the fluid excitation force on the pump should be computed at first. We combined the CFD/FEM/BEM technique to predict the pump vibration and sound radiation under fluid excitation. The complicated fluid force was extracted and set as a boundary condition for the FEM, BEM solution, and the coupled FEM-BEM algorithm.

The contents of this paper are organized as follows. Section 2 introduces the experimental setup in this study. Section 3 presents the CFD model and methodology. Section 4 provides the volute structural and acoustical simulation methods. Section 5 first provides the comparison between the results from the two approaches and experimental data and then presents the discussions of the effects of the outlet width on hydraulically generated vibration and noise.

2. Experimental Setup

In this study, a single entry, single volute centrifugal pump with 5 blades was used as the experimental machine. The impeller is designed to operate at 2900 rpm. The designed flow rate is 50 m^3/h, and the designed head is 30 m. And its corresponding specific speed n_q(SI) is 26.7. The study comprises four impellers with different outlet width. These impellers will be termed A, B, C, and D, respectively. General pump geometric values for A, B, C, and D are identified in Table 1.

The experiments were carried out in a close hydraulic test rig, as shown in Figure 1. A more detailed description of the test facility and the experimental procedure can be found in our previous work [28]. In present study, the vibration measurements are carried out by using four PCB 352A60 accelerometers with the sensitivity of 10 mv/(m/s^2). These accelerometers were fixed on four positions of the volute exterior surface, as shown in Figure 2.

Table 1: Main pump parameters.

Parameter	Description	Value
d_1 (m)	Inlet diameter of impeller	0.036
d_2 (m)	Outlet diameter of impeller	0.168
z (—)	Number of blades	5
β_2 (°)	Outlet blade angle	33
γ (°)	Total blade wrap angle	115
b_{2A} (m)	Impeller outlet width of Impeller A	0.006
b_{2B} (m)	Impeller outlet width of Impeller B	0.008
b_{2C} (m)	Impeller outlet width of Impeller C	0.01
b_{2D} (m)	Impeller outlet width of Impeller D	0.012
d_3 (m)	Radius to cutwater	0.184
b_3 (m)	Volute width	0.02
d_4 (m)	Discharge nozzle diameter	0.05

3. Fluid Simulation

The pump model details are exposed in [28]. Figure 3 presents an example of the mesh and the interfaces of the pump. The commercial software CFX was applied to solve the transient fully 3D Reynolds-averaged Navier-Stokes equations in the whole pump. Turbulence was simulated with a k-ω SST model. The standard wall function was used to calculate boundary layer variables. In the study, the y^+ on the impeller and volute surfaces is well below 16, satisfying the requirements of the turbulence model and wall function. The boundary conditions are set as a constant total pressure at the inlet and a mass flow rate at the outlet. The transient calculations were initialized from the steady solutions. The average residual convergence criterion was set to be 1E-5. The CFD results were recorded after five impeller revolutions to achieve a stabilized solution. The simulations in this study were carried out on a cluster of twelve Intel Xeon 5600 nodes. The grid dependence study was carried out through five grid topologies. Further details about the CFD model can be found in our previous work [28].

4. Volute Structural and Acoustical Simulation Method

The methods for vibration and sound simulation used in the study are illustrated in Figure 4. The approaches consist of the following steps.

① The fluid model and structure model are prepared.

② CFD computation is carried out by using CFX and the nonlinear fluid excitation force on the pump is stored in a time-series.

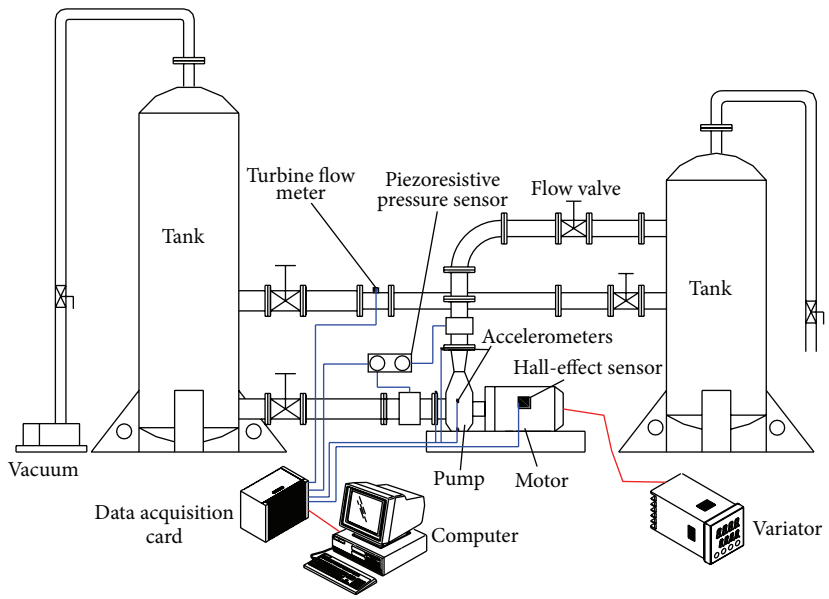

Figure 1: A close hydraulic test rig.

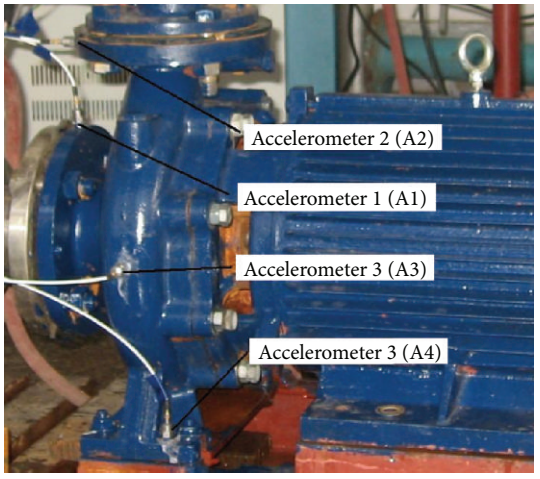

Figure 2: Location of the accelerometers.

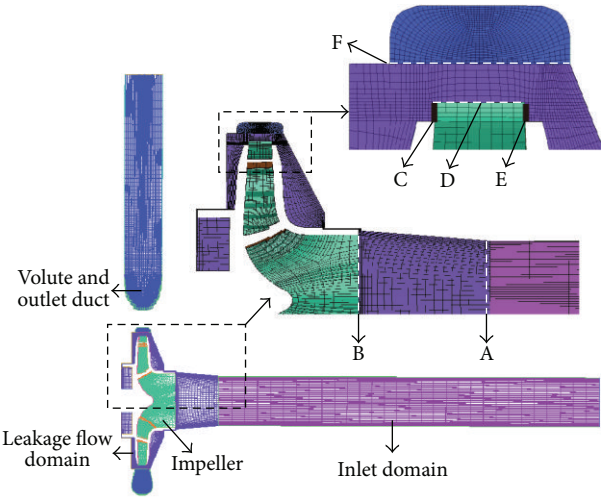

Figure 3: Details of pump mesh and interfaces.

③ The structure model is imported into Ansys software. The modal analysis is carried out under constraint.

④ The time-series fluid excitation force is imported into Ansys by using the APDL tool in the software. The time-series force is treated as the boundary condition. And the structure response is simulated.

Steps (①)~(④) are the FEM analyses for vibration.

⑤ The outer surface of the pump structure is extracted and meshed, which is treated as BEM mesh for acoustic simulation.

⑥ The BEM mesh is imported into the Sysnoise software. The pump structure response and modal data are imported into the Sysnoise software.

⑦ Define the sound material properties and constraint.

⑧ In Sysnoise, the normal velocity distribution on the outer surface nodes of the structure is transferred to the surface nodes of the BEM model.

⑨ The vibration velocity data on the BEM mesh is set as boundary condition, and then the acoustic simulation is carried out by using Sysnoise.

Steps (⑤)~(⑨) are the BEM analyses for acoustic. But for the coupled FEM-BEM algorithm, more steps are need on the basis of steps (①)~(⑨). For the coupled method, the additional steps are as follows.

⑩ Import the FEM mesh into the Sysnoise software.

⑪ Define the solid material properties and constraint for the FEM model in Sysnoise.

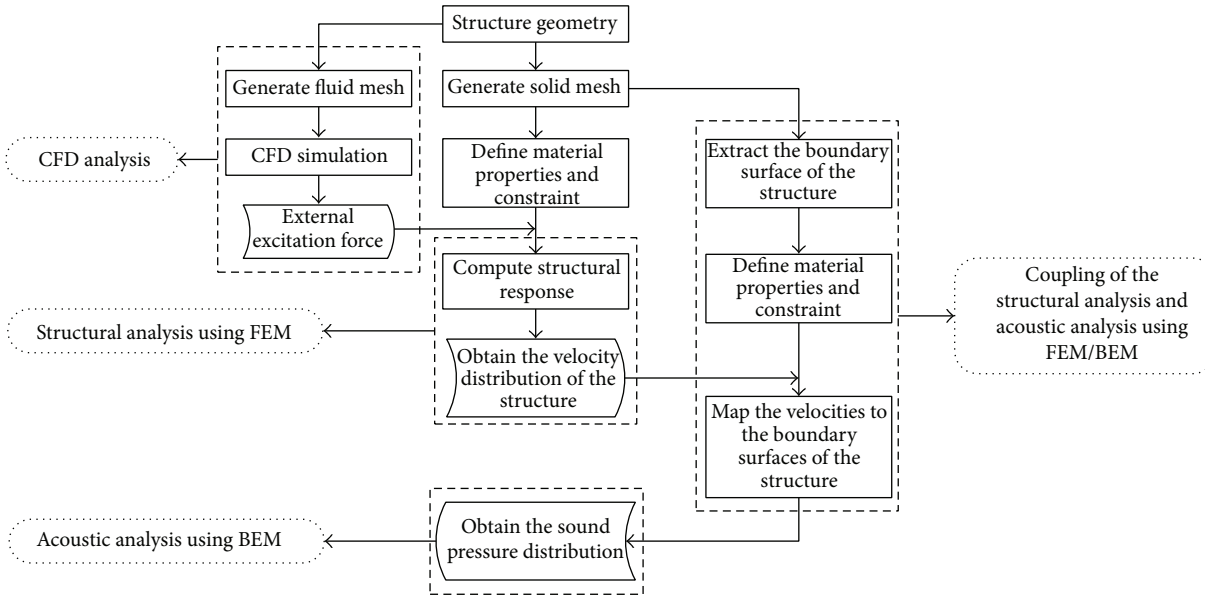

Figure 4: Volute structural and acoustical simulation method.

⑫ In the software Sysnoise, the pump outer surface is treated as a coupled surface. This surface is used to exchange data between the FEM model and BEM model. In this case, the coupled surface is the same with the BEM mesh;

⑬ Calculate the response of the coupled surface under vibration excitation from the FEM model and sound pressure excitation from the BEM model.

From the contents mentioned above, the difference between the two approaches is that the coupling surface between the FEM model and BEM model was built in the coupled FEM-BEM methods in order to consider the feedback effects of the sound pressure on the pump structure.

4.1. Volute Vibration Simulation Method. The equation that governs the dynamic response of the structure can be written in the following form:

$$[\mathbf{M}]\left\{\ddot{\delta}\right\} + [\mathbf{C}]\left\{\dot{\delta}\right\} + [\mathbf{K}]\{\delta\} = \{\mathbf{P}(\mathbf{t})\}, \tag{1}$$

where $[\mathbf{M}]$ is the mass matrix, $[\mathbf{C}]$ is the damping matrix, $[\mathbf{K}]$ is the stiffness matrix, $\{\boldsymbol{\delta}\}$ is the nodal structural displacement vector, and $\{\mathbf{P}(\mathbf{t})\}$ is the external excitation force vector applied on the nodal structure which is a function of time. The damping matrix $[\mathbf{C}]$ can be a linear combination of the stiffness and mass matrices according to Rayleigh's theory. The formula is

$$[\mathbf{C}] = \alpha[\mathbf{M}] + \beta[\mathbf{K}], \tag{2}$$

where α, β represent the mass and stiffness proportional damping constants, respectively. The two constants can be given as a function of the natural frequency and the damping ratio, as the following equations:

$$\alpha = \frac{2\left(\zeta_i w_j - \zeta_j w_i\right)}{\left(w_j + w_i\right)\left(w_j - w_i\right)} w_i w_j,$$
$$\beta = \frac{2\left(\zeta_j w_j - \zeta_i w_i\right)}{\left(w_j + w_i\right)\left(w_j - w_i\right)}, \tag{3}$$

where w_i and w_j are the ith and jth mode natural frequency, respectively; ζ_i and ζ_j are the ith and jth mode damping ratio, respectively. In present study, both modes are assumed to have the same damping ratio ($\zeta = \zeta_i = \zeta_j$) and the damping ratio was estimated to be 0.04 [29, 30]; then; (3) can be written as

$$\alpha = \zeta \frac{2 w_i w_i}{\left(w_i + w_j\right)} \qquad \beta = \zeta \frac{2}{\left(w_i + w_j\right)}. \tag{4}$$

The excitation force $\{\mathbf{P}(\mathbf{t})\}$ is calculated by transferring the hydrodynamic load on the CFD mesh to the structure mesh. To realize this process, a discrete data transfer including three steps was developed in this study, as shown in Figure 5. Step 1 is mesh searching used to find matching CFD surface elements for each structure node, which can be very time-consuming. To get over this problem, a bucket algorithm developed by Bonet and Peraire [31] was used to reduce the search complexity. The step 2 is mesh matching, which is to find a nearest CFD mesh element to a structure mesh node. The CFD mesh shape can be defined as

$$\mathbf{N}_j^{\mathbf{E}}(\varepsilon, \eta) = \sum_i \mathbf{r}_{i,j}^{\mathbf{E}} \mathbf{B}_i(\varepsilon, \eta), \tag{5}$$

where $\mathbf{r}_{i,j}^{\mathbf{E}}$ represents CFD mesh element nodes, $\mathbf{B}_i(\varepsilon, \eta)$ is the element basis functions, and (ε, η) is the CFD mesh element

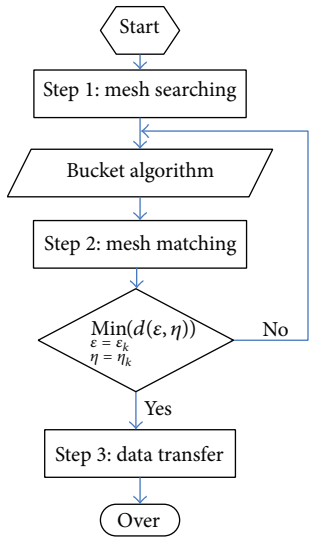

Figure 5: Data transfer between fluid and structure mesh.

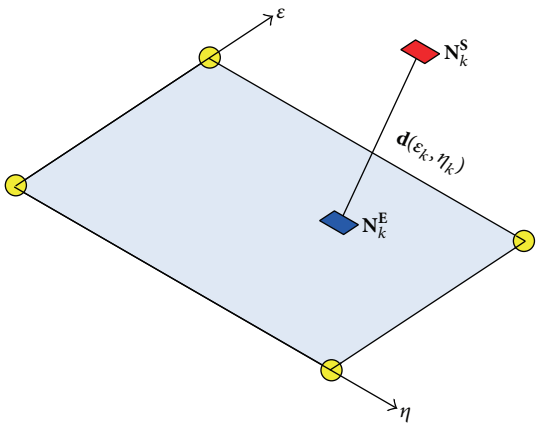

Figure 6: Relation between the source and target meshes.

coordinates. The surface elements for CFD calculations are quadrilateral, as shown in Figure 6. The distance from a structure node ($\mathbf{N}_k^{\mathbf{S}}$) to any node on the CFD mesh element can be written in the following formula:

$$\mathbf{d}(\varepsilon,\eta) = \left\| \mathbf{N}_k^{\mathbf{S}} - \sum_i \mathbf{r}_{i,j}^{\mathbf{E}} \mathbf{B}_i(\varepsilon,\eta) \right\|. \tag{6}$$

The nearest CFD mesh element node (ε_k, η_k) should meet the following equation:

$$\min_{\substack{\varepsilon=\varepsilon_k \\ \eta=\eta_k}} (d(\varepsilon,\eta)) \Longrightarrow \begin{cases} \dfrac{\partial d}{\partial \varepsilon|_{\varepsilon=\varepsilon_k}} = 0 \\ \dfrac{\partial d}{\partial \eta|_{\eta=\eta_k}} = 0. \end{cases} \tag{7}$$

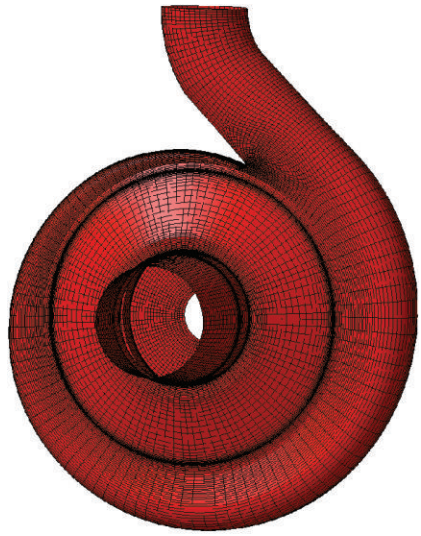

Figure 7: Source mesh of the volute.

Step 3 is the data transfer from fluid surface elements to structure nodes. The data transfer function was defined as [32]

$$p_k^{\mathbf{S}}(\varepsilon_k,\eta_k) = \sum_i p_i^{\mathbf{E}} \mathbf{B}_i(\varepsilon_k,\eta_k), \tag{8}$$

where $p_i^{\mathbf{E}}$ is the pressure on the CFD mesh element nodes and $p_k^{\mathbf{S}}(\varepsilon_k,\eta_k)$ is the pressure transferred from fluid to the structure nodes. Figure 7 shows the CFD mesh used in the data transfer process. Figure 8 presents the structure mesh of the pump volute, which consists of 59201 elements and 15785 nodes.

The material used in the simulation is iron, with the properties elastic module $E = 211$ GPa, the density $\rho = 7870\ \mathrm{kg/m^3}$, the poisson ration $\nu = 0.29$. The excitation force $\{\mathbf{P}(\mathbf{t})\}$ was set as the boundary condition. The constraints were imposed as follows: the nodes of the foundation bolt hole were completed fixed, with $u_x = u_y = u_z = 0$; the displacement of nodes on the bearing holes was $u_x = u_y = u_z = 0$; $u_z = 0$ on the inlet flanges; $u_x = 0$ on the outlet flanges. The boundary set was shown in Figure 8.

4.2. Volute Acoustic Simulation. The boundary element method (BEM) in the Sysnoise software was applied to perform the volute acoustic simulation. The governing equation for radiated sound pressure in the surrounding air induced by vibration of the volute structure can be written in the following form:

$$c(\mathbf{r})p(\mathbf{r}) = \int_{\Omega} \left\{ p(\mathbf{r}_0) \frac{\partial \mathbf{G}(\mathbf{r},\mathbf{r}_0)}{\partial \mathbf{n}} + iw\rho_0 \mathbf{u}_{\mathbf{n}}(\mathbf{r})\, \mathbf{G}(\mathbf{r},\mathbf{r}_0) \right\} d\Omega, \tag{9}$$

where $\mathbf{r}$ is a position vector of receiver, $\mathbf{r}_0$ is a position vector on the boundary surface, $p(\mathbf{r}_0)$ is acoustic pressure on the boundary surface, $iw\rho_0 \mathbf{u}_{\mathbf{n}}(\mathbf{r})$ is the surface normal

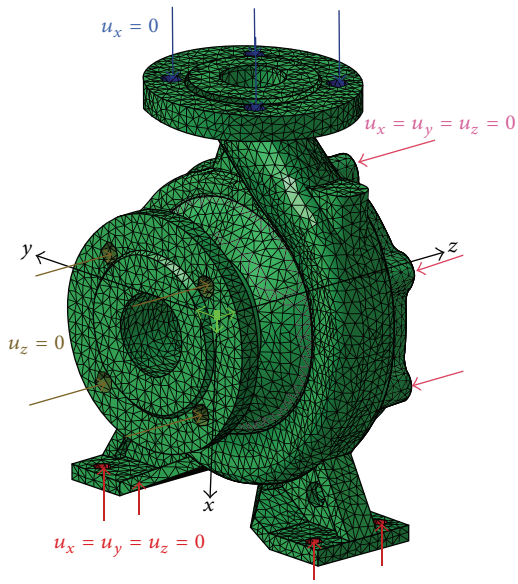

Figure 8: Structure mesh of the volute.

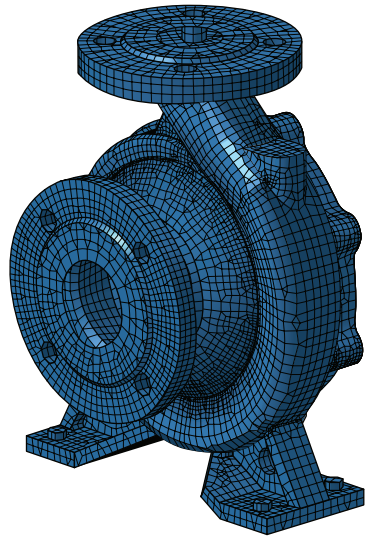

Figure 9: Acoustic mesh of the volute.

acceleration, $c(\mathbf{r})$ is a geometry related coefficient, $c(\mathbf{r}) = 0.5$ if $\mathbf{r} \in \boldsymbol{\Omega}$, $c(\mathbf{r}) = 1$ if $\mathbf{r} \in \mathbf{V} - \boldsymbol{\Omega}$, and $c(\mathbf{r}) = 0$ if $\mathbf{r} \notin \mathbf{V}$. $\mathbf{G}(\mathbf{r},\mathbf{r}_0)$ is Green's function, which can be written in the following form:

$$\mathbf{G}\left(\mathbf{r},\mathbf{r}_0\right) = \frac{e^{-ik|\mathbf{r}-\mathbf{r}_0|}}{4\pi\left|\mathbf{r}-\mathbf{r}_0\right|}. \tag{10}$$

The outer surface of the structure was extracted and meshed as the acoustic model used in the BEM calculation, as shown in Figure 9. The acoustical mesh consists of 14706 elements and 13573 nodes. As the maximum valid frequency of the model investigated in this study was 4366 Hz, the mesh was sufficiently fine for the blade passing frequency (242 Hz), according to the literature [33]. The normal velocity distribution on the outer surface nodes of the structure was transferred to the surface nodes of the acoustic model, which was set as the boundary condition of the volute acoustic simulation. Then, the sound pressure distribution was solved by using the BEM method.

4.3. Volute Structural-Acoustic Coupling Simulation Method. The acoustic solution is carried out by (9). Considering the effect of the sound pressure on the structural vibration, (1) can be written in the following form:

$$[\mathbf{M}]\left\{\ddot{\delta}\right\} + [\mathbf{C}]\left\{\dot{\delta}\right\} + [\mathbf{K}]\{\delta\} + \left[\mathbf{L_c}\right]\left\{\mathbf{p}\left(\mathbf{r}_0\right)\right\} = \left\{\mathbf{P}\left(\mathbf{t}\right)\right\}, \tag{11}$$

where $[\mathbf{M}]$ is the mass matrix, $[\mathbf{C}]$ is the damping matrix, $[\mathbf{K}]$ is the stiffness matrix, $\{\boldsymbol{\delta}\}$ is the nodal structural displacement vector, $\{\mathbf{P}(\mathbf{t})\}$ is the external excitation force vector, and $[\mathbf{L_c}]\{\mathbf{p}(\mathbf{r_0})\}$ is the load applied on the structure nodes by the sound pressure. The $[\mathbf{L_c}]$ is the coupling matrix, which is defined as

$$\left[\mathbf{L_c}\right] = -\sum_{e=1}^{n_{se}}\left(\int_{\Omega}\left(\mathbf{N}_k^{\mathbf{S}}\{n^e\}\,\mathbf{N}_l^{\mathbf{A}}\right)d\Omega\right), \tag{12}$$

where $\mathbf{N}_k^{\mathbf{S}}$ is the structure mesh shape function, $\mathbf{N}_l^{\mathbf{A}}$ is the acoustic mesh shape function, $\{n^e\}$ is the normal direction of the coupling surface elements, and n_{se} is the number of the coupling surface elements.

5. Results and Discussions

The vibration and noise induced by inner flow in the pump with different impeller outlet width were analyzed and compared at three flow conditions. Before the numerical methods were used, the simulation results were validated by the vibration acceleration of the monitoring points. The detailed analyses and discussions are as follows.

5.1. Experimental Validation. In this experiment, the noise measurements were not carried out because of a shortage of the anechoic chamber. However, the vibration measurements were used to validate the two methods mentioned above. Figure 10 presents the measured spectra of vibration accelerations of the measuring points. It is found that the synchronous vibration at the shaft frequency Ω of 48 Hz dominates the low frequencies. This can be caused by the excitations from the mechanical unbalance, hydraulic unbalance, bent rotor, and excessive run-out of components. There are noticeable peaks at 3Ω and 4Ω due to loose parts, loose bearing, or rubbing. The peaks at the blade passing frequency (BPF) 5Ω are clearly visible in the figure. The BPF vibrations are excited by the rotor-stator interaction. The peak at labeled ① represents the discharge pipe resonance excited by high pressure pulsation at the pump outlet. It is observed that the vibration measurements of the sampling point A2 are greatly affected by the discharge pipe resonance, which may lead to great errors. In order to validate the two simulation approaches, the measured vibration accelerations under the flow condition $\Phi = 0.162$ were used and compared with the simulation results, as shown in Figure 10. As can be seen from this figure, there are no significant differences between

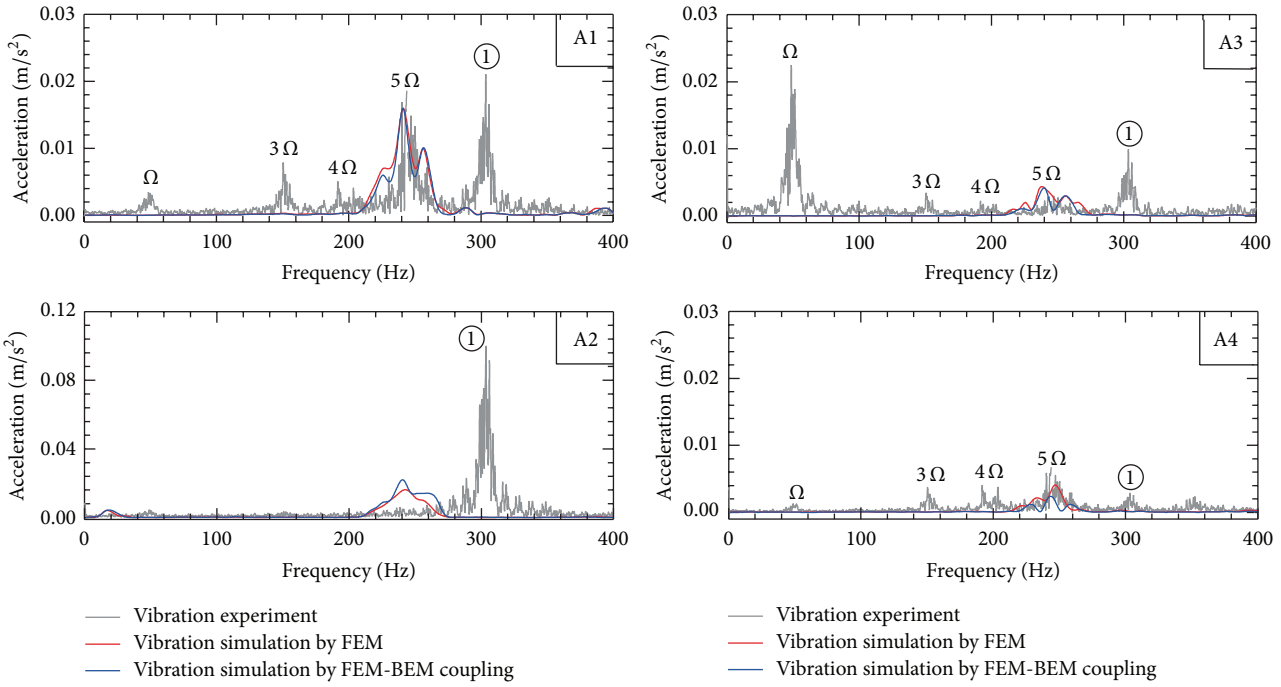

Figure 10: Comparisons between measured and calculated spectra of vibration acceleration of the monitoring points.

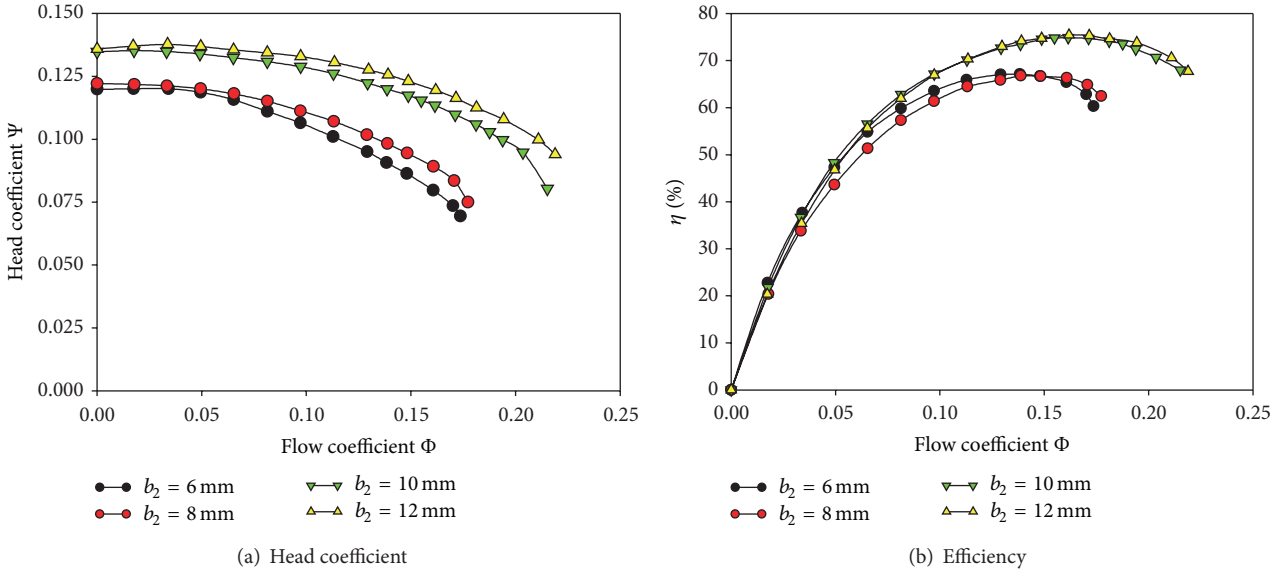

(a) Head coefficient (b) Efficiency

Figure 11: Performance comparisons between the four pumps with different outlet width.

the two vibration simulation approaches. This indicated the influences of the noise of centrifugal pumps on the structure appear insignificant. It is found that the BPF amplitudes at the points A1, A3, and A4 show good agreements with the experimental results. However, at the low frequency components and the ① component, the differences between the measured and calculated results are relatively large. That is because the behaviors of the rotor and pipe resonance have been neglected. In the simulation only the dynamic surface pressure on the walls is used. As such, the following discussions focus on the BPF component.

5.2. Performance Comparisons. Through the experiments, the detailed performance of the four pumps with different impeller outlet width is obtained. Figures 11(a) and 11(b) present the performance comparisons between the four pumps. According to Figure 11(a), the head coefficient increases with the increase of impeller outlet width. A big raise of the head and efficiency is observed when the impeller outlet width changes from 8 mm to 10 mm. This indicates the impeller with outlet width $b_2 = 10$ mm is more suitable for the pump. As can be seen from Figure 11(b), there are no significant changes of the efficiency between the pump with

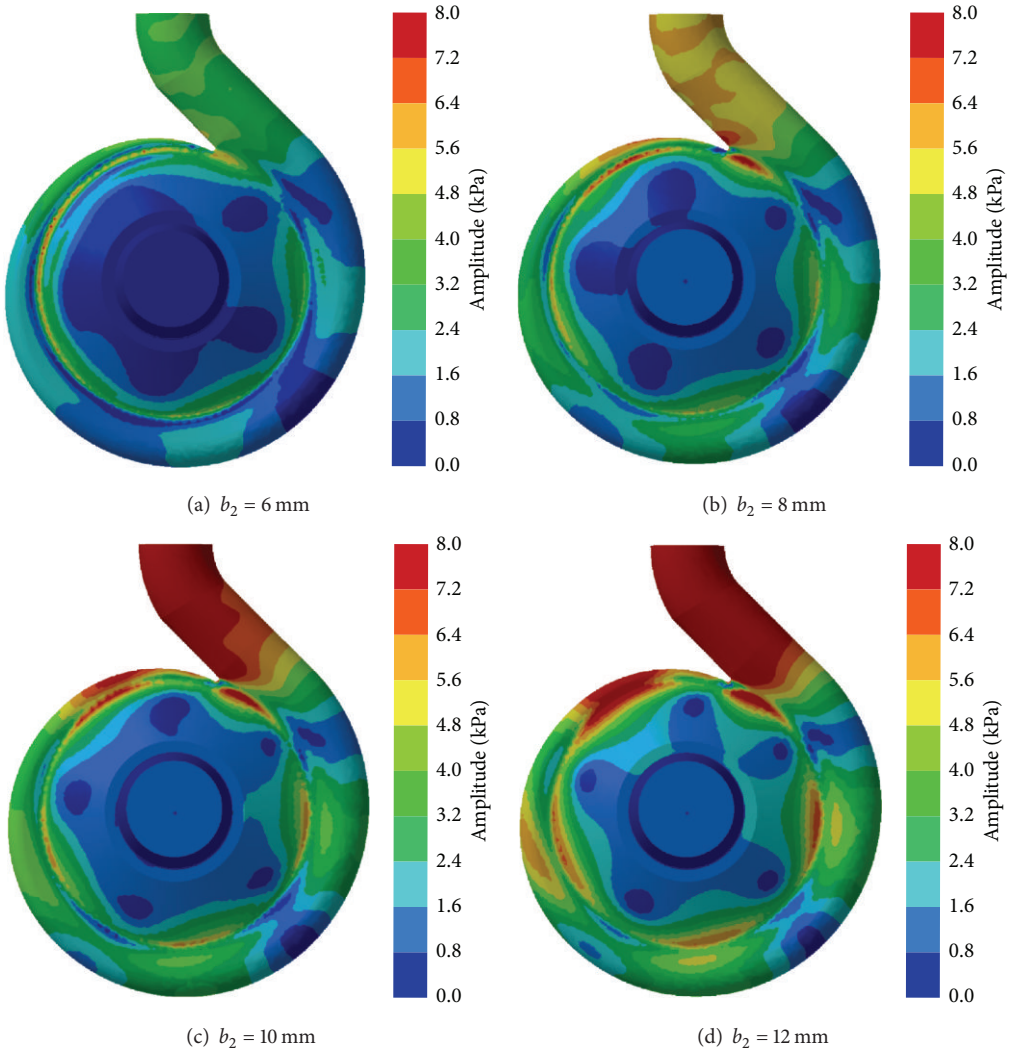

(a) $b_2 = 6$ mm (b) $b_2 = 8$ mm

(c) $b_2 = 10$ mm (d) $b_2 = 12$ mm

Figure 12: Pressure amplitudes at BPF on the casing wall under flow condition $\Phi = 0.162$.

$b_2 = 10$ mm and $b_2 = 12$ mm. This is because a sufficiently large outlet width is likely to cause a big increase of the nonuniformity of the flow at the impeller outlet. This can cause more turbulent dissipation losses in the volute.

5.3. Pressure Pulsation on the Casing Wall. The pressure on the casing wall obtained by the CFD calculations was processed by using the Fast Fourier Transform with a Hanning Window. Figure 12 presents the amplitudes of the pressure pulsations at BPF on the casing wall. According to the results, the pressure amplitudes increase with growing outlet width. When the impeller outlet width increases, the nonuniformity of the flow at the impeller outlet gets increased, causing higher pressure pulsations. Significant high levels of pressure amplitudes are mainly detected in three regions, including the region around the tongue, the diffuser wall, and the second hydraulic profile of the volute. This is due to the effect of the blade-tongue interaction at BPF. At BPF, the blade trailing edge just passes the tongue leading edge, which causes strong pressure pulsations around the tongue region. When the impeller outlet width increases, the excessive pressure pulsations at the tongue region propagate into the diffuser and the collector along the flow path. Large vibration displacements are to be expected at these regions because of the excessive pressure pulsations. Figures 13(a) and 13(b) show the pressure amplitudes at BPF under the flow conditions $\Phi = 0.097$ and $\Phi = 0.130$, respectively. It can be found that the pressure pulsations at the second profile get larger with decreasing flow rates. And the pressure pulsations around the tongue regions get larger with growing flow rates. This phenomenon will cause great changes in vibration levels at the two regions over the flow rates.

5.4. Volute Structural Vibration Simulation. Figure 14 presents the vibration velocity at BPF under the flow condition $\Phi = 0.162$. It can be found that the largest vibration

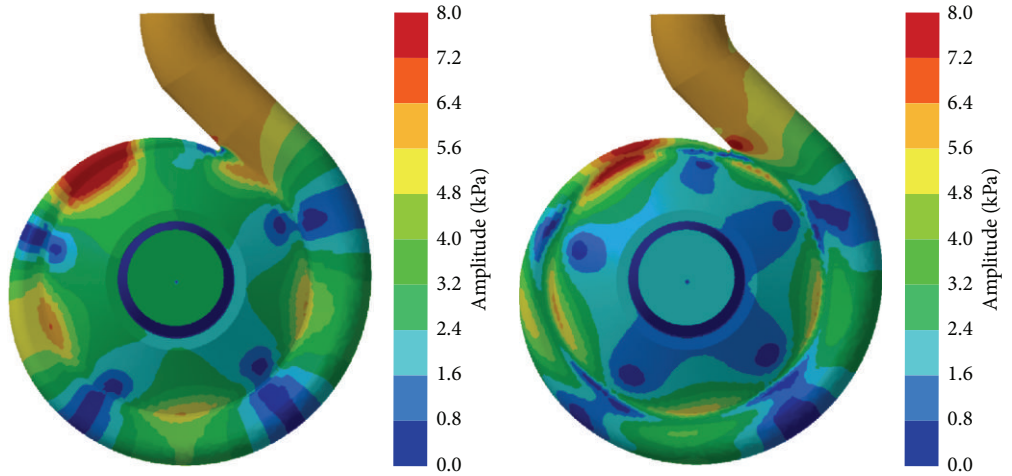

(a) $\Phi = 0.097$ (b) $\Phi = 0.130$

FIGURE 13: Pressure amplitudes at BPF with $b_2 = 8$ mm under flow conditions (a) $\Phi = 0.097$ and (b) $\Phi = 0.130$.

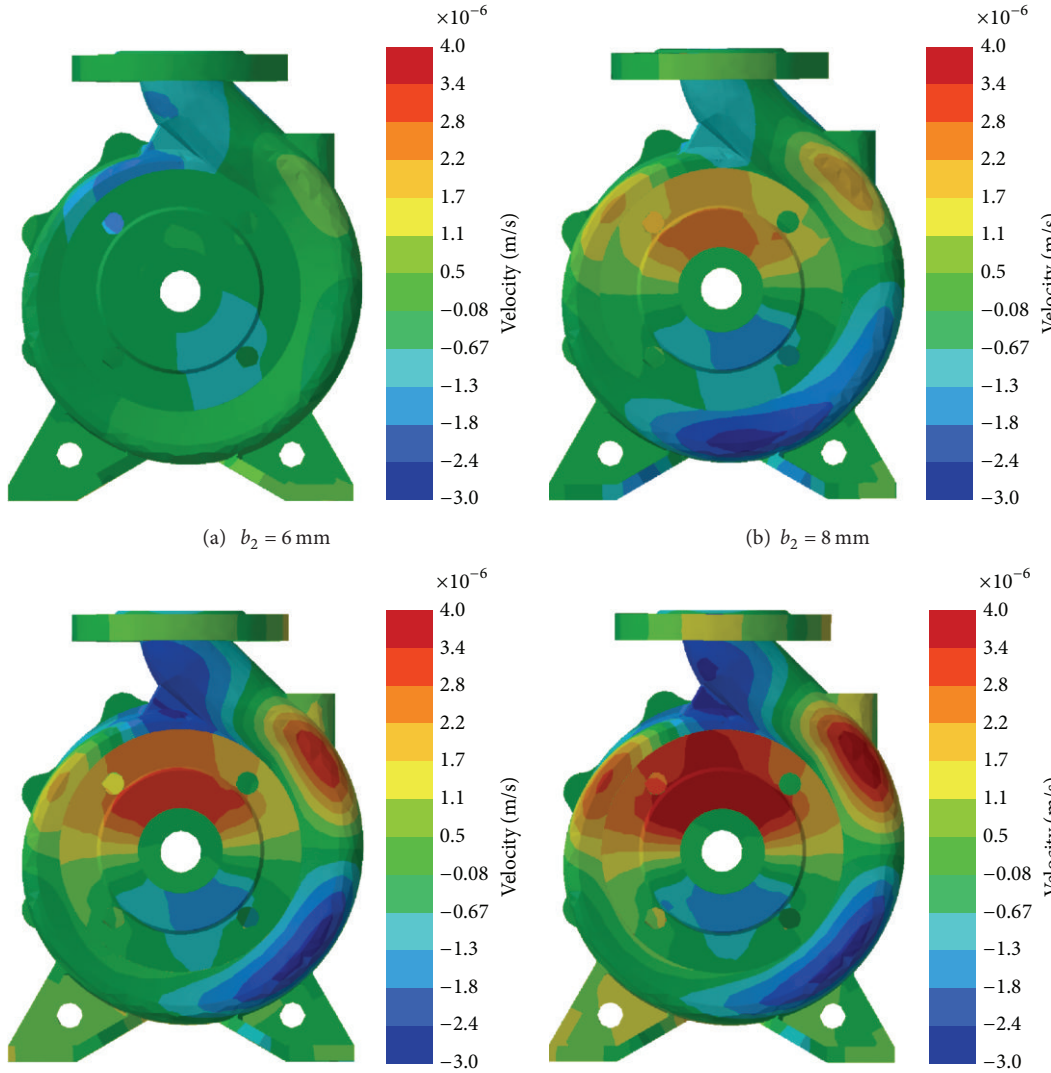

(a) $b_2 = 6$ mm (b) $b_2 = 8$ mm

(c) $b_2 = 10$ mm (d) $b_2 = 12$ mm

FIGURE 14: Vibration velocity at BPF under flow condition $\Phi = 0.162$.

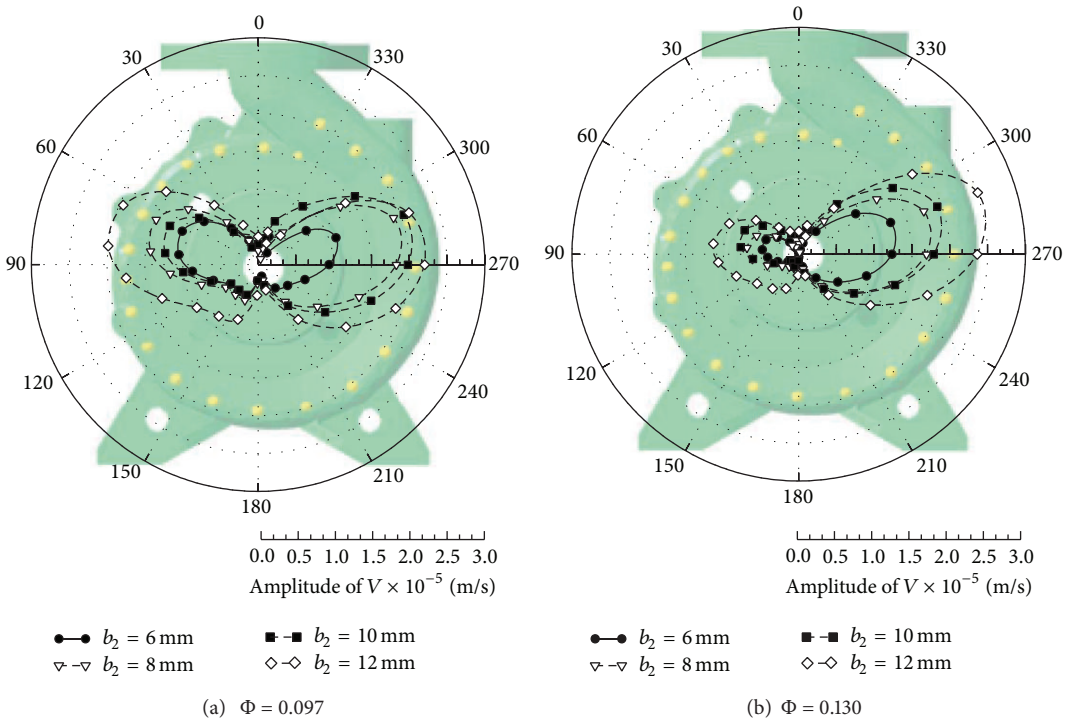

Figure 15: Amplitudes of the vibration velocity at BPF under flow conditions (a) Φ = 0.097 and (b) Φ = 0.130.

velocities take place at six regions. These regions include the region around the tongue, the diffuser wall, the second and the sixth as well as the eighth hydraulic profile of the volute, and the inlet flange. These regions are expected because of the high pressure pulsations according to Figure 12. Also, an appreciable rise of the vibration velocity is clearly visible when the impeller outlet width increases. Figures 15(a) and 15(b) show the velocity amplitudes at BPF under the flow conditions Φ = 0.097 and Φ = 0.130, respectively. In the figures, the angular coordinate represents the circumferential position of the monitoring points (yellow points located in a circle on the casing wall shown in this figure), and the radial coordinate represents the amplitudes of the vibration velocity in y-direction. It can be found that there are two peaks of the velocity amplitudes occurring at the second and eighth hydraulic profile of the volute. As can be seen from Figure 15, obvious reduction at the second hydraulic profile is clearly visible with the increase of the flow rate. This is because the pressure pulsations at the second profile of the volute decreases with growing flow rates according to Figure 13. Also, an appreciable rise of the velocity amplitude is clearly visible when the impeller outlet width increases.

5.5. Volute Acoustic Simulation. A spherical acoustic mesh of radius 0.5 m with the volute at its center was used to calculate the directivity distribution of the sound pressure level that radiated from the pump. Figure 16 shows the sound pressure level at BPF under the flow condition Φ = 0.162. It can be found that as the impeller outlet width increases, the sound pressure level increases, with the maximum magnitude in the vertical direction. The big noise in the vertical direction is caused by the high amplitudes of the pressure pulsations and vibration level at the pump outlet regions. Figures 17(a) and 17(b) show the directivity distributions of the sound pressure level at BPF under the flow conditions Φ = 0.097 and Φ = 0.130, respectively. It is found that the sound pressure level increases with decreasing flow rates. This corresponds with the influence of the flow rates on the pressure pulsations and the vibration. As can be seen from Figure 17, although the sound pressure level increased due to the increase of the impeller outlet width, the SPL value of the pump with b_2 = 10 mm is much larger than the others. This indicates that the impeller outlet width should be selected under a certain level. In this case, the level is expected to be less than 10 mm, corresponding to the relative outlet width b_2^* (b_2/d_2) of 0.06. According to the literature, the relative outlet width b_2^* is commonly selected from empirical data. The b_2^* at n_q(SI) = 26.7 is 0.083 according to the literature [3]. And, when the b_2^* exceeds 0.06, the pump losses are extremely large, according to the performance comparisons in Figure 11. Therefore, the relative outlet width b_2^* at n_q(SI) = 26.7 in this paper should be less than 0.06, based on an overall consideration of the pump characteristics, pressure pulsations, vibration and noise level.

6. Conclusion

The effects of the impeller outlet width on the hydraulically generated vibration and noise of a centrifugal pump volute were studied. For this purpose, two approaches were used to predict the vibration and sound radiation of the volute under fluid excitation. Before the numerical methods were used, the simulation results were validated by the vibration acceleration

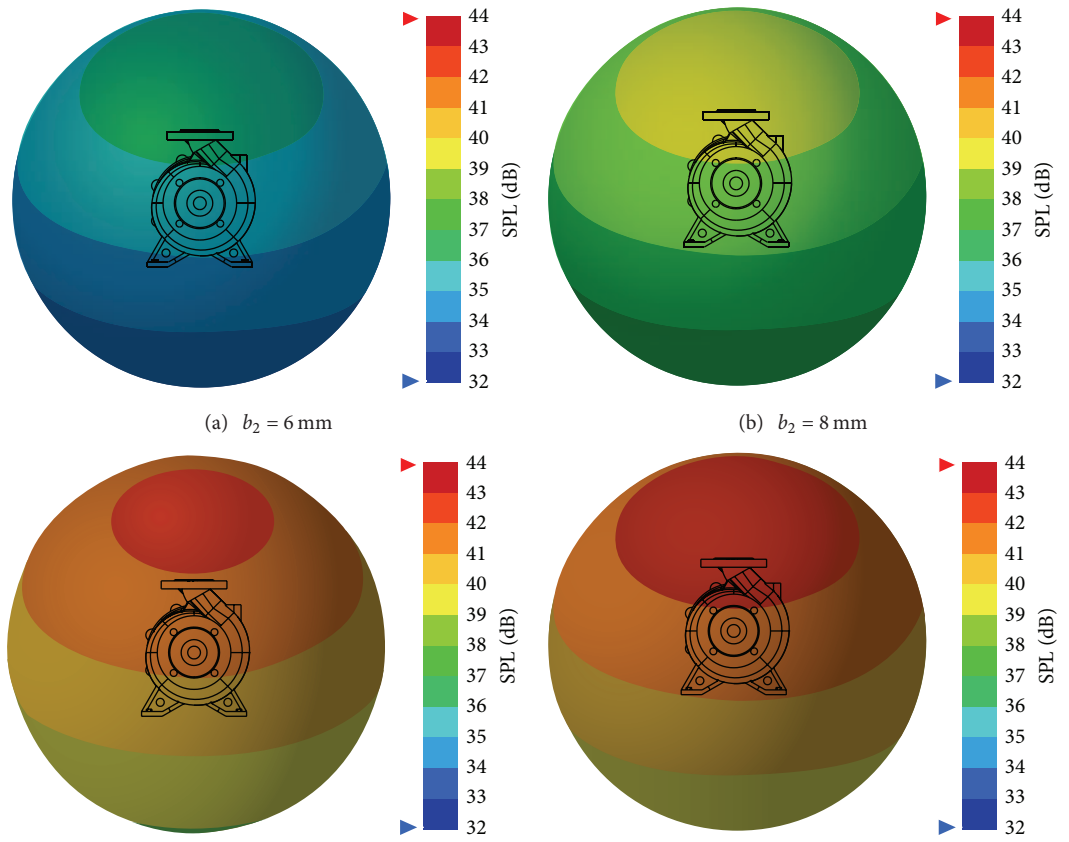

(a) $b_2 = 6$ mm (b) $b_2 = 8$ mm

(c) $b_2 = 10$ mm (d) $b_2 = 12$ mm

Figure 16: Sound pressure level at BPF under flow condition $\Phi = 0.162$.

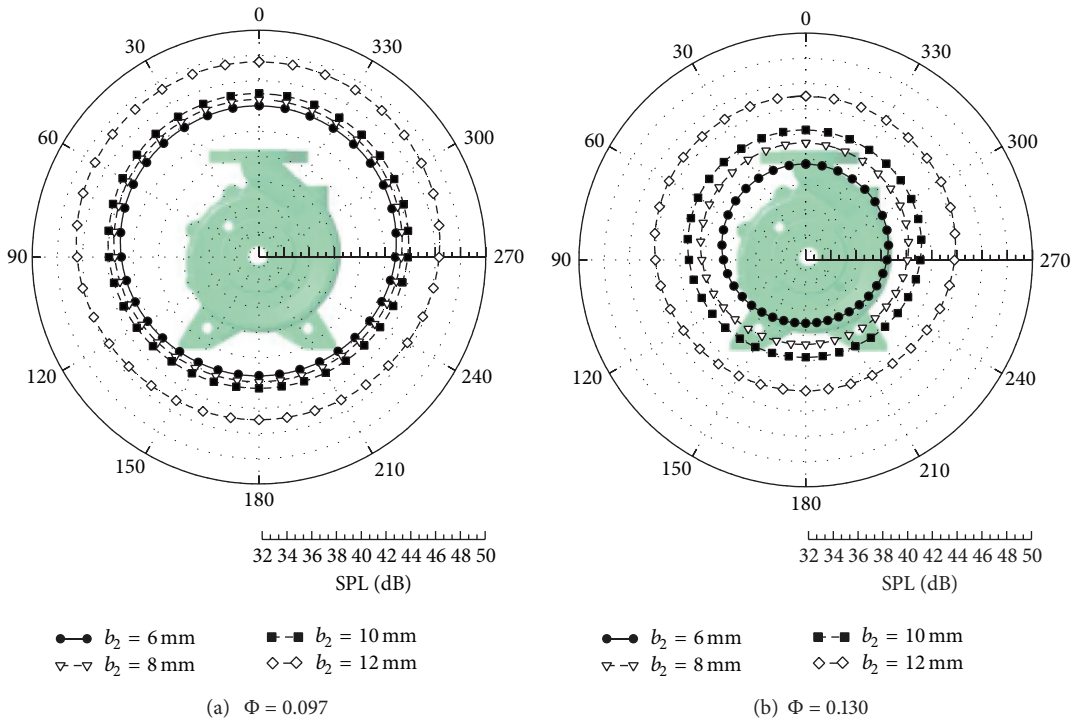

(a) $\Phi = 0.097$ (b) $\Phi = 0.130$

Figure 17: Directivity distributions of the SPL at BPF under flow conditions (a) $\Phi = 0.097$ and (b) $\Phi = 0.130$.

of the monitoring points on the volute. The vibration and noise were analyzed and compared at three flow conditions. The analysis of the results gives the following conclusions.

(1) The combined CFD/FEM simulation method and the combined CFD/FEM/BEM structural-acoustic coupling method are compared. The results indicate that the influences of the sound pressure of centrifugal pumps on the structure appear insignificant.

(2) The BPF magnitudes of the pressure pulsations, vibration, and noise level of the centrifugal pump volute get increased with growing impeller outlet width, with the maximum value occurring at six regions. The regions with high vibration velocity appear at the tongue area, the pump outlet, the second and the sixth as well as the eighth hydraulic profile of the volute, and the inlet flange. The region with high SPL mainly appear at the pump outlet in the vertical direction. The high BPF magnitudes at these regions are related to the distributions of pressure pulsations on the casing wall caused by the stator-rotor interaction. Furthermore, the BPF magnitudes are increased significantly when the impeller outlet width exceeds a certain level. In this study, the level is $b_2 = 10$ mm. The relative outlet width b_2^* at $n_q(\mathrm{SI}) = 26.7$ in this paper should be less than 0.06, based on an overall consideration of the pump characteristics, pressure pulsations, vibration and noise level.

Nomenclature

d_1: Inlet diameter of impeller, m
d_2: Outlet diameter of impeller, m
z: Number of blades
b_2: Outlet width of impeller, m
b_2^*: Relative outlet width
d_3: Radius to cutwater, m
b_3: Volute width, m
d_4: Discharge nozzle diameter, m
Q: Flow rate, designed flow rate, m^3/h
H: Head, designed head, m
n: Rotation speed, r/min
y^+: Dimensionless distance from the wall
BPF: Blade passing frequency, Hz.

Greek Letters

β_2: Outlet blade angle, $\circ$
γ: Total blade wrap angle, $\circ$
Ω: Shaft frequency, Hz
Ψ: Head coefficient, $gH/(\Omega^2 d_2^2)$
Φ: Flow coefficient, $Q/(3600\Omega b_2 d_2^2)$
η : Pump efficiency, %.

Subscripts

1: Impeller inlet
2: Impeller outlet.

Conflict of Interests

All authors declare no conflict of interests.

Acknowledgment

This work was sponsored by the National Natural Science project of China (no. 51109095, 51179075), PAPD and the Jiangsu Province project (no. CXZZ13_0675).

References

[1] B. Dürrer, F. H. Wurm, and W. Ag, "Noise sources in centrifugal pumps," in *Proceedings of the 2nd WSEAS Int. Conference on Applied and Theoretical Mechanics*, pp. 203–207, Venice, Italy, 2006.

[2] R. Birajdar, R. Patil, and K. Khanzode, "Vibration and noise in centrifugal pumps sources and diagnosis methods," in *Proceedings of the 3rd International Conferences on Integrity, Reliability and Failure*, Porto, Portugal, July 2009.

[3] J. F. Gulich, *Centrifugal Pumps*, Springer, 2010.

[4] S. S. Rudnev and V. A. Khabetskaya, "Selection of width of a pump impeller at its outlet," *Chemical and Petroleum Engineering*, vol. 16, no. 9, pp. 545–549, 1980.

[5] W. Shi, L. Zhou, W. Lu, B. Pei, and T. Lang, "Numerical prediction and performance experiment in a deep-well centrifugal pump with different impeller outlet width," *Chinese Journal of Mechanical Engineering*, vol. 26, no. 1, pp. 46–52, 2013.

[6] L. Zhou, W. Shi, and S. Wu, "Performance optimization in a centrifugal pump impeller by orthogonal experiment and numerical simulation," *Advances in Mechanical Engineering*, vol. 2013, Article ID 385809, 7 pages, 2013.

[7] C. H. Simpson, R. Macaskill, and T. A. Clark, "Generation of hydraulic noise in centrifugal pumps," *Proceedings of the Institution of Mechanical Engineers, Conference Proceedings*, vol. 181, pp. 84–108, 1966.

[8] H. C. Simpson, T. A. Clark, and G. A. Weir, "A theoretical investigation of hydraulic noise in pumps," *Journal of Sound and Vibration*, vol. 5, no. 3, pp. 456–488, 1967.

[9] P. H. Bent, *Experiments on the aerodynamic generation of noise in centrifugal turbomachinery [Ph.D. thesis]*, The Pennsylvania State University, 1993.

[10] S. Chu, R. Dong, and J. Katz, "Relationship between unsteady flow, pressure fluctuations, and noise in a centrifugal pump part A: use of PDV data to compute the pressure field," *Journal of Fluids Engineering, Transactions of the ASME*, vol. 117, no. 1, pp. 24–29, 1995.

[11] S. Chu, R. Dong, and J. Katz, "Relationship between unsteady flow, pressure fluctuations, and noise in a centrifugal pump—part B: effects of blade-tongue interactions," *Journal of Fluids Engineering*, vol. 117, no. 1, pp. 30–35, 1995.

[12] G. Rzentkowski, "Generation and control of pressure pulsations emitted from centrifugal pumps: a review," in *Proceedings of the ASME Pressure Vessels and Piping Conference (PVP '96)*, PVP-1996, pp. 328–439, Montreal, Canada, July 1996.

[13] M. Morgenroth and D. S. Weaver, "Sound generation by a centrifugal pump at blade passing frequency," *Journal of Turbomachinery*, vol. 120, no. 4, pp. 736–743, 1998.

[14] R. Dong, S. Chu, and J. Katz, "Effect of modification to tongue and impeller geometry on unsteady flow, pressure fluctuations,

and noise in a centrifugal pump," *Journal of Turbomachinery*, vol. 119, no. 3, pp. 506–515, 1997.

[15] G. Rzentkowski and S. Zbroja, "Experimental characterization of centrifugal pumps as an acoustic source at the blade-passing frequency," *Journal of Fluids and Structures*, vol. 14, no. 4, pp. 529–558, 2000.

[16] J.-S. Choi, D. K. McLaughlin, and D. E. Thompson, "Experiments on the unsteady flow field and noise generation in a centrifugal pump impeller," *Journal of Sound and Vibration*, vol. 263, no. 3, pp. 493–514, 2003.

[17] S. Berten, M. Farhat, P. Dupont, and F. Avellan, "Rotor-stator interaction induced pressure fluctuations: CFD and hydroacoustic simulations in the stationary components of a multistage centrifugal pump," in *Proceedings of the 5th Joint ASME/JSME Fluids Engineering Summer Conference (FEDSM '07)*, pp. 963–970, San Diego, Calif, USA, August 2007.

[18] C. Kato, M. Kaiho, and A. Manabe, "An overset finite-element large-eddy simulation method with applications to turbomachinery and aeroacoustics," *Journal of Applied Mechanics*, vol. 70, no. 1, pp. 32–43, 2003.

[19] W.-H. Jeon and D.-J. Lee, "A numerical study on the flow and sound fields of centrifugal impeller located near a wedge," *Journal of Sound and Vibration*, vol. 266, no. 4, pp. 785–804, 2003.

[20] M. A. Langthjem and N. Olhoff, "A numerical study of flow-induced noise in a two-dimensional centrifugal pump. Part I: hydrodynamics," *Journal of Fluids and Structures*, vol. 19, no. 3, pp. 349–368, 2004.

[21] M. A. Langthjem and N. Olhoff, "A numerical study of flow-induced noise in a two-dimensional centrifugal pump, Part II: hydroacoustics," *Journal of Fluids and Structures*, vol. 19, no. 3, pp. 369–386, 2004.

[22] C. Kato, Y. Yamade, H. Wang et al., "Numerical prediction of sound generated from flows with a low Mach number," *Computers & Fluids*, vol. 36, no. 1, pp. 53–68, 2007.

[23] S.-Q. Yuan, Q.-R. Si, F. Xue, J. Yuan, and J. Zhang, "Numerical calculation of internal flow induced noise in centrifugal pump volute," *Journal of Drainage and Irrigation Machinery Engineering*, vol. 29, no. 2, pp. 93–98, 2011.

[24] C. Kato, Y. Yamade, H. Wang et al., "Prediction of the noise from a multi-stage centrifugal pump," in *Proceedings of the ASME Fluids Engineering Division Summer Meeting (FEDSM '05)*, vol. 1, pp. 1273–1280, Houston, Texas, USA, June 2005.

[25] Y. Y. Jiang, S. Yoshimura, R. Imai, H. Katsura, T. Yoshida, and C. Kato, "Quantitative evaluation of flow-induced structural vibration and noise in turbomachinery by full-scale weakly coupled simulation," *Journal of Fluids and Structures*, vol. 23, no. 4, pp. 531–544, 2007.

[26] S. A. Eftekhari and A. A. Jafari, "A mixed modal-differential quadrature method for free and forced vibration of beams in contact with fluid," *Meccanica*, vol. 49, no. 3, pp. 535–564, 2014.

[27] T. Opperwall and A. Vacca, "A combined FEM/BEM model and experimental investigation into the effects of fluid-borne noise sources on the air-borne noise generated by hydraulic pumps and motors," *Proceedings of the Institution of Mechanical Engineers Part C: Journal of Mechanical Engineering Science*, vol. 228, no. 3, pp. 457–471, 2014.

[28] H. Liu, J. Ding, H. Dai, and M. Tan, "Investigation into transient flow in a centrifugal pump with wear ring clearance variation," *Advances in Mechanical Engineering*, vol. 2014, Article ID 693097, 15 pages, 2014.

[29] W. D. Marscher, "An end-user's guide to centrifugal pump rotordynamics," in *Proceedings of the 23rd Pump Users Symposium*, pp. 69–93, 2007.

[30] F. T. Kaiser, H. R. Osman, and R. O. Dickau, "Analysis guide for variable frequency drive operated centrifugal pumps," in *Proceedings of the 24th International Pump User's Symposium*, pp. 81–106, Texas A&M University, Texas, Tex, USA, 2008.

[31] J. Bonet and J. Peraire, "An alternating digital tree (ADT) algorithm for 3D geometric searching and intersection problems," *International Journal for Numerical Methods in Engineering*, vol. 31, no. 1, pp. 1–17, 1991.

[32] J. A. Samareh, "Discrete data transfer technique for fluid-structure interaction," AIAA Paper AIAA-2007-4309, 2007.

[33] S. Marburg, "Six boundary elements per wavelength: is that enough?" *Journal of Computational Acoustics*, vol. 10, no. 1, pp. 25–51, 2002.